
Unified Molecular Modeling via Modality Blending

Qiyong Yu¹ Yudi Zhang² Yuyan Ni³ Shikun Feng¹ Yanyan Lan¹
Hao Zhou^{1*} Jingjing Liu¹

¹ Institute for AI Industry Research, Tsinghua University

² Harbin Institute of Technology

³ Academy of Mathematics and Systems Science, Chinese Academy of Sciences

Abstract

Self-supervised molecular representation learning is critical for molecule-based tasks such as AI-assisted drug discovery. Recent studies consider leveraging both 2D and 3D information for representation learning, with straightforward alignment strategies that treat each modality separately. In this work, we introduce a novel "blend-then-predict" self-supervised learning method (*MoleBLEND*), which blends atom relations from different modalities into one unified relation matrix for encoding, then recovers modality-specific information for both 2D and 3D structures. By treating atom relationships as anchors, seemingly dissimilar 2D and 3D manifolds are aligned and integrated at fine-grained relation-level organically. Extensive experiments show that *MoleBLEND* achieves state-of-the-art performance across major 2D/3D benchmarks. We further provide theoretical insights from the perspective of mutual-information maximization, demonstrating that our method unifies contrastive, generative (inter-modal prediction) and mask-then-predict (intra-modal prediction) objectives into a single cohesive *blend-then-predict* framework.

1 Introduction

Self-supervised learning has been successfully applied to molecular representation learning [60, 65, 13, 77], where meaningful representations are extracted from a large amount of unlabeled molecules and can be finetuned to support diverse downstream molecular tasks. Early works design learning objectives based on a single modality (2D topological graphs, or 3D spatial structures). There are two main schools of 2D methods: generative approach [28, 49], which masks and reconstructs substructures of 2D graphs; and contrastive method [54, 70, 63, 69, 62], which learns invariant molecular graph representations. Recent 3D methods use proxy tasks of recovering corrupted 3D information (e.g., coordinates [74, 35, 78, 29], atom types [78], bond lengths and angles [18]) to learn pretrained models, which have achieved remarkable performance on molecular property prediction tasks. Effective as they are on current benchmarks, calculating molecules' 3D geometry at scale required by real-world applications [21] is computationally intractable [53, 3].

Multimodal molecular representation learning [36, 53, 34, 39, 79], which exploits both 2D and 3D modalities in a single framework, has also emerged as an effective solution, by marrying the capability of processing 2D graphs with utilizing critical 3D information in an efficient manner. Most existing methods use contrastive learning on two separate modality-specific (2D or 3D) models [36, 53, 34], which attracts representations of 2D graphs with their corresponding 3D conformations of the same molecule, and repulse those from different molecules. Another avenue is generative method that takes 2D graphs as input to predict 3D information and vice versa [36, 79, 34].

*Corresponding Author

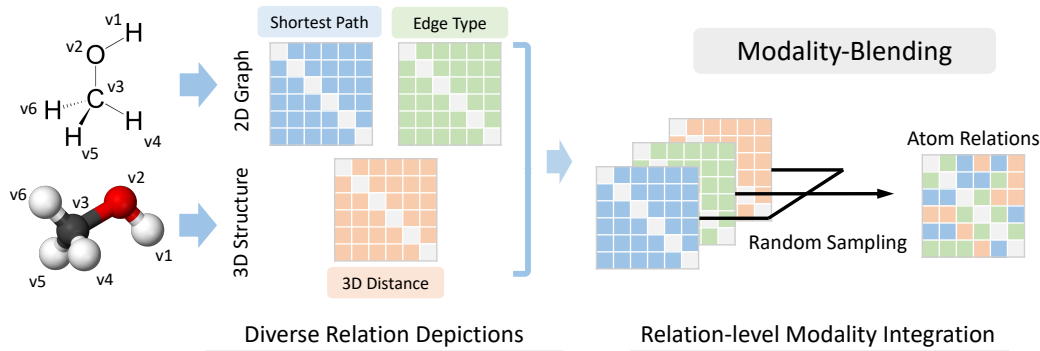


Figure 1: Illustrations of Modality-Blending. Same atoms (v_1, \dots, v_6) are shared across modalities, while the depictions of atom relationships (shortest path, edge type, 3D distance) are represented by different matrices, which are blended into an integral input for unified pretraining.

Although appearing visually distinct and residing in different high-dimensional manifold spaces, 2D molecular graphs and 3D spatial structures both represent the same underlying structures, *i.e.*, *atoms* and their *relationships*, whereas all existing works explicitly distinguish these different modalities as independent signals and treat them as separate inputs. As 2D and 3D structures are essentially different manifestations of the same molecule, merely regarding them as separate inputs loses the inherent connection between amorphous atomic relations. Instead, information from different modalities should be modeled jointly from the very beginning, rather than being treated separately. In addition, existing contrastive learning approaches aim to align different modalities only on a coarse-grained level. [73, 66] show that contrastive learning used in CLIP [45] and image pretraining [11] lacks detailed structural understanding. This limitation also manifests in the context of molecules, where existing contrastive learning methods obtain representations only on the molecule level while missing a deep structural comprehension of the constituting atoms within the molecule. This may exert adverse impact because the missing detailed information plays a vital role in representing atomic constituents and their intricate relations [51, 38]. Thus, a fine-grained alignment between different modalities is needed to better integrate diverse atomic-relation representations.

In this work, we advocate for *unified molecular modeling* with an organic *fine-grained* integration of 2D and 3D modalities. We propose to blend all modalities into one integral input to a single backbone model for pretraining. This is a non-trivial practice because different modalities exhibit heterogeneous data forms (e.g., molecular graphs vs. 3D spatial structures) that are inherently difficult to mingle together. However, although appearing distinct across modalities (e.g., shortest path and edge type on 2D graphs, Euclidean distance in 3D space), atom relations can be viewed as the same properties described by diverse forms. We thus leverage atom relations as the anchor to blend different modalities into a single unified data structure ($n \times n$ matrix) (Figure 1). In this way, our approach aligns the fundamentally identical yet visually dissimilar 2D and 3D manifolds at a fine-grained relation-level, aiming at modeling intrinsic molecular properties in a cohesive manner.

Specifically, we introduce a novel self-supervised learning method, *MoleBLEND*, consisting of two *blend-then-predict* steps: modality-blended encoding and modality-targeted prediction. During encoding, we leverage atom relations as the anchor to bridge modalities, and blend different depictions of atom relations from multiple modalities into one relation matrix. Notably, our model takes partial 2D and 3D information as input (without overlapping sub-structures), different from all existing methods that take in full 2D or 3D relations for either contrastive or generative objectives [36, 53, 39, 34]. During prediction, the model recovers 2D and 3D information as supervision signals. With such a blend-then-predict approach, multimodal molecular information are modeled within a unified model, and the relation-level fine-grained alignment leads to a deep structural understanding of molecules. Extensive experiments demonstrate that the proposed modality-blending method achieves state-of-the-art performance across a broad range of 2D and 3D benchmarks. We provide further theoretical insights from the perspective of mutual-information maximization to explain the blend-then-predict process, which essentially unifies existing contrastive [53], generative [36] (inter-modal prediction), and mask-then-predict (intra-modal prediction) objectives into one unified objective formulation.

2 Related Work

Multimodal molecular representation learning [36, 53, 79, 39, 34] leverages both 2D and 3D information to enhance molecular representations and bears a trade-off between cost and performance, as 3D information is vital for molecular property prediction while 3D models tend to be resource-intensive during deployment. Most existing methods utilize two separate models to encode 2D and 3D information [36, 53, 34]. Their pretraining methods mostly use contrastive learning [24, 9, 22, 10, 45, 8, 72, 75, 45, 71], which treats 2D graphs with their corresponding 3D conformations as positive views and information from different molecules as negative views for contrasting [36, 53, 34]. Another school of pretraining methods uses generative models to predict one modality based on the input of another modality [36, 34]. [79] proposes to encode both 2D and 3D inputs within a single GNN model, by either treating atom type and edge type as vertex and edge (2D input), or taking coordinates and distance as vertex and edge (3D input), during training. Although single model is used here, different modalities are still processed separately. We instead propose to leverage atom relations as the anchor, to blend representations from different modalities into one single matrix as an integral input for the single model.

Masked Auto-Encoding [59] is a widely applied technique for representation learning [6, 17, 37, 5, 67, 12, 61, 19, 55]. This strategy follows a conceptually simple *mask-then-predict* paradigm that removes a portion of the data and learns to predict the missing content, such as in BERT [15] and MAE [23]. Our proposed *blend-then-predict* framework is inherently congruent with this ethos, by first masking and blending information across modalities, then learning to recover the complete data. Essentially, it can be regarded as a multimodal version of masked auto-encoding.

3 Unified Molecular Representation Learning

Molecules are typically represented by either 2D molecular graph or 3D spatial structure. Despite their distinct appearances, they depict a common underlying structure, *i.e.*, atoms and their relationships (*e.g.*, shortest path distance and edge type in 2D molecular graph, and Euclidean distance in 3D structure). Naturally, these representations should be unified organically, instead of treated separately with different models, in order to learn the representation of complex chemical relations underneath. This belief serves as a north star in guiding our design of a fine-grained objective to unified molecular representation learning, as well as the design of backbone architecture.

3.1 Problem Formulation

A molecule \mathcal{M} can be represented as a set of atoms $\mathcal{V} \in \mathbb{R}^{n \times v}$ along with their relationships $\mathcal{R} \in \mathbb{R}^{n \times n \times r}$, where n is the number of atoms, v and r are dimensions of atom and relation feature, respectively. The nature of \mathcal{R} can vary depending on the context. In the commonly used 2D graph representation of molecules, \mathcal{R} is represented by the chemical bonds \mathcal{E} , which are the edges of the 2D molecular graph. In 3D scenarios, \mathcal{R} is defined as the relative Euclidean distance \mathcal{D} between atoms.

To leverage both 2D and 3D representations, we adopt the shortest path distance \mathcal{R}_{spd} and the edge type encoding $\mathcal{R}_{\text{edge}}$ of molecular graph, as well as Euclidean distance $\mathcal{R}_{\text{distance}}$ in 3D space, as three different appearances of atom relations across 2D/3D modalities. And instead of treating each modality separately with individual models, we blend the three representations into a single matrix $\mathcal{R}_{2\text{D}\&3\text{D}}$ by randomly sampling each representation for each vector, following a pre-defined multinomial distribution S . Our pre-training objective is to maximize the following likelihood:

$$\max \mathbb{E}_S P(\mathcal{R}_{\text{spd}}, \mathcal{R}_{\text{edge}}, \mathcal{R}_{\text{distance}} | \mathcal{R}_{2\text{D}\&3\text{D}}, \mathcal{V}) \quad (1)$$

We employ the Transformer model [58] to parameterize our objective, capitalizing on its ability to incorporate flexible atom relations in a fine-grained fashion through attention bias [46, 52, 30, 68]. This choice is further supported by recent research demonstrating that a single Transformer model can effectively process both 2D and 3D data [39].

Transformer Block The Transformer architecture is composed of a stack of identical blocks, each containing a multi-head self-attention layer and a position-wise feed-forward network. Residual connection [25] and layer normalization [4] are applied to each layer. Denote $\mathbf{X}^l = [\mathbf{x}_1^l; \mathbf{x}_2^l; \dots; \mathbf{x}_n^l]$ as the input to the l -th block with the sequence length n , and each vector $x_i \in \mathbb{R}^d$ is the contextual

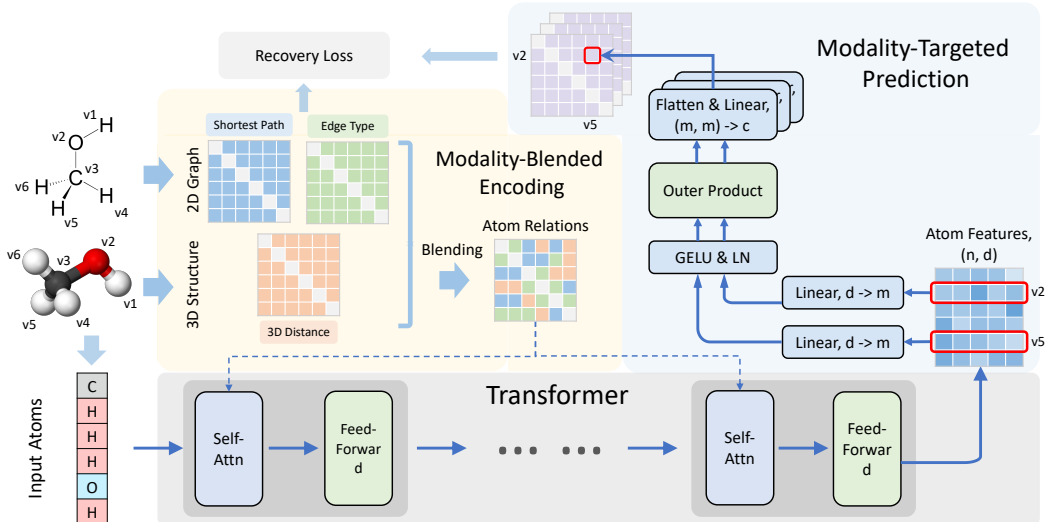


Figure 2: Illustration of unified molecular representation learning process, consisting of two steps: 1) modality-blended encoding, which blends diverse atom relations together and injects it into the self-attention module of Transformer for unified cross-modality encoding; 2) modality-targeted prediction, where atom features encoded by Transformer are transformed into atom relations through an outer product projection module, to recover the diverse relation depictions.

representation of the atom at position i . d is the dimension of the hidden representations. A Transformer block first computes the multi-head self-attention to effectively aggregate the input sequence \mathbf{X}^l :

$$\text{Multi-Head}(\mathbf{X}) = \text{Concat}(\text{head}_1, \dots, \text{head}_h) \mathbf{W}^O \quad (2)$$

where $\text{head}_i = \text{Attention}(\mathbf{X}\mathbf{W}_i^Q, \mathbf{X}\mathbf{W}_i^K, \mathbf{X}\mathbf{W}_i^V)$ and h is the number of attention heads. $\mathbf{W}_i^Q, \mathbf{W}_i^K, \mathbf{W}_i^V \in \mathbb{R}^{d \times d_h}$, $\mathbf{W}^O \in \mathbb{R}^{d \times d}$ are learnable parameter matrices. The attention computation is defined as:

$$\text{Attention}(\mathbf{Q}, \mathbf{K}, \mathbf{V}) = \text{softmax}\left(\frac{\mathbf{Q}\mathbf{K}^\top}{\sqrt{d}}\right) \mathbf{V} \quad (3)$$

Generally, given input X^l , the l -th block works as follows:

$$\tilde{\mathbf{X}}^l = \text{LayerNorm}(\mathbf{X}^l + \text{Multi-Head}(\mathbf{X}^l)) \quad (4)$$

$$\mathbf{X}^{l+1} = \text{LayerNorm}(\tilde{\mathbf{X}}^l + \text{GELU}(\tilde{\mathbf{X}}^l \mathbf{W}_1^l) \mathbf{W}_2^l) \quad (5)$$

where $\mathbf{W}_1^l \in \mathbb{R}^{d \times d_f}$, $\mathbf{W}_2^l \in \mathbb{R}^{d_f \times d}$, and d_f is the intermediate size of the feed-forward layer.

3.2 Learning Objective

To achieve unified modeling of molecules that facilitates organic integration of different depictions of atoms and their relations across 2D/3D spaces, we design a new ‘blend-then-predict’ training paradigm that consists of two steps: 1) modality-blended encoding that encodes a molecule with blended information from different modalities; and 2) modality-targeted prediction that recovers the original 2D and 3D input. The pre-training process is illustrated in Figure 2. The core idea is to bind different modalities together at a granular level by blending relations from multiple modalities into an integral input from the get-go, to encourage the model to discover fundamental and unified relation representations across heterogeneous forms.

Modality-blended Encoding Multimodal learning aims to learn the most essential representations of data that possess inherent connections while appearing distinctive between different modalities. In the context of molecules, atom relationships are the common attributes underpinning different

representations across 2D/3D modalities. This motivates us to leverage relations as anchors, to align both modalities in a fine-grained manner that blends multimodalities from the very beginning.

We adopt three appearances of relations across 2D and 3D modalities: shortest path distance, edge type, and 3D Euclidean distance. For each atom pair (i, j) , Ψ_{SPD}^{ij} represents the shortest path distance between atom i and j . We encode the edge features along the shortest path between i and j as the edge encoding, $\Psi_{\text{Edge}}^{ij} = \frac{1}{N} \sum_{n=1}^N \mathbf{w}_n^\top \mathbf{e}_n$, where $(\mathbf{e}_1, \mathbf{e}_2, \dots, \mathbf{e}_N), \mathbf{e}_n \in \mathbb{R}^{d_e}$ are features of edges on the shortest path between i and j . $w_n \in \mathbb{R}^{d_e}$ are learnable parameters. Following [78, 39], we encode Euclidean distances of an atom pair (i, j) with Gaussian Basis Kernel function [50]:

$$\zeta_k^{ij} = \mathcal{G}(\mathcal{A}(d^{ij}; \gamma^{ij}, \beta^{ij}); \mu_k, \sigma_k), k = 1, \dots, K \quad (6)$$

$$\Psi_{\text{Distance}}^{ij} = \text{GELU}(\zeta^{ij} \cdot W_{3\text{D}}^1) W_{3\text{D}}^2, \zeta^{ij} = [\zeta_1^{ij}, \dots, \zeta_K^{ij}]^\top \quad (7)$$

where $\mathcal{A}(d; \gamma, \beta) = \gamma \cdot d + \beta$ is the affine transformation with learnable parameters γ and β , and $\mathcal{G}(d; \mu, \sigma) = \frac{1}{\sqrt{2\pi}\sigma} \exp\left(-\frac{1}{2\sigma^2} (d - \mu)^2\right)$ is the Gaussian density function with parameters μ and σ . K is the number of Gaussian Basis kernels. $W_{3\text{D}}^1 \in \mathbb{R}^{K \times K}, W_{3\text{D}}^2 \in \mathbb{R}^{K \times 1}$ are learnable parameters. $\Psi_{\text{SPD}}, \Psi_{\text{Edge}}, \Psi_{\text{Distance}}$ denote the three relation matrices of all atom pairs, with the same shape $n \times n$.

Different from existing works that separately feed one of these relations into different models, we blend them together from the get-go and randomly mix them into one relation matrix, which is then fed into one single model for molecule encoding. Specifically, we first define a multinomial distribution S with a probability vector $p = (p_1, p_2, p_3)$. For each position (i, j) in the matrix, we draw a sample $s^{ij} \in \{1, 2, 3\}$ following the probability distribution p , then determine the corresponding element of the blended matrix as follows:

$$\Psi_{2\text{D}\&3\text{D}}^{ij} = \Psi_{\text{SPD}}^{ij} \mathbb{1}_1 + \Psi_{\text{Edge}}^{ij} \mathbb{1}_2 + \Psi_{\text{Distance}}^{ij} \mathbb{1}_3, \text{ where } \mathbb{1}_k = \begin{cases} 1 & \text{if } s^{ij} = k \\ 0 & \text{otherwise} \end{cases} \quad (8)$$

, where each position (i, j) randomly selects its element from one of the $\Psi_{\text{SPD}}^{ij}, \Psi_{\text{Edge}}^{ij}, \Psi_{\text{Distance}}^{ij}$. After the process finishes, distinct relation manifestations $(\Psi_{\text{SPD}}, \Psi_{\text{Edge}}, \Psi_{\text{Distance}})$ across modalities are blended into a single modality-blended matrix $\Psi_{2\text{D}\&3\text{D}} \in \mathbb{R}^{n \times n}$ without overlapping sub-structures, to represent the inter-atomic relations.

We inject this *modality-blended* relation $\Psi_{2\text{D}\&3\text{D}}$ into the self-attention module, which captures pair-wise relations between inputs atoms, to provide complementary pair-wise information. This practice is also similar to the relative positional encoding for Transformer [46]:

$$\text{Attention}(\mathbf{Q}, \mathbf{K}, \mathbf{V}) = \text{softmax}\left(\frac{\mathbf{Q}\mathbf{K}^\top}{\sqrt{d}} + \Psi_{2\text{D}\&3\text{D}}\right) \mathbf{V} \quad (9)$$

With modality-blending, we bind different modalities together at fine-grained relation level for molecule encoding, which will help the model better integrate information from multimodalities.

Modality-targeted Prediction The model recovers the full $\mathcal{R}_{\text{spd}}, \mathcal{R}_{\text{edge}}$ and $\mathcal{R}_{\text{distance}}$ as its training objectives. The intuition is, if the model can predict different types of atom relations, like shortest path on the molecular graph or 3D Euclidean distance, given a *single mixed representation*, this cross-modality representation must have captured some underlying integral molecular structure.

Specifically, after modality-blended encoding, we obtain contextual atom representations $\mathbf{X}^{L+1} \in \mathbb{R}^{n \times d}$ encoded by an L -layer Transformer. We propose an outer product projection module to transform the atom representations into $n \times n$ atom relations. The representations \mathbf{X}^{L+1} are first linearly projected to a smaller dimension $m = 32$ with two independent Linear layers $\mathbf{W}_l, \mathbf{W}_r \in \mathbb{R}^{m \times d}$. The outer products are computed upon the transformed representations, which are then flattened and projected into the target space with a modality-targeted head $\mathbf{W}_{\text{head}} \in \mathbb{R}^{c \times m^2}$. The relation computation between the i -th and j -th atoms is formulated as follows:

$$\mathbf{o}_{ij} = \mathbf{G}(\mathbf{W}_l \mathbf{X}_i^{L+1}) \otimes \mathbf{G}(\mathbf{W}_r \mathbf{X}_j^{L+1})^\top \in \mathbb{R}^{m \times m} \quad (10)$$

$$\mathbf{z}_{ij} = \mathbf{W}_{\text{head}} \cdot \text{Flatten}(\mathbf{o}_{ij}) \in \mathbb{R}^c \quad (11)$$

where $\mathbf{G}(\cdot) = \text{LayerNorm}(\text{GELU}(\cdot))$. We now obtain the modality-targeted relation matrix $\mathbf{Z} \in \mathbb{R}^{n \times n \times c}$, where c depends on the targeted task. The predictions of shortest path distance and edge

type are formulated as classification tasks, where c is the number of possible shortest path distance or edge types. For predicting 3D distance, we formulate it as a 3-dimensional regression task, and the regression targets are the relative Euclidean distances in 3D space.

Noisy Node as Regularization Noisy node [20, 74, 39] incorporates an auxiliary loss for coordinate denoising in addition to the original objective, which has been found effective in improving representation learning. We also adopt this practice as an additional regularization term, by adding Gaussian noise to the input coordinates and requiring the model to predict the added noise.

3.3 Finetuning

The trained model can be finetuned to accept both 2D and 3D inputs for downstream tasks. For scenarios where a large amount of 2D molecular graphs is available while 3D conformations are too expensive to obtain, the model can take only 2D input to finetune the model. Formally, given shortest path distance \mathcal{R}_{spd} , edge type $\mathcal{R}_{\text{edge}}$ and atom types \mathcal{V} as available 2D information, we define $\mathbf{y}_{2\text{D}}$ as the task target, K as the number of training samples, and $\ell(\cdot, \cdot)$ as the loss function of the specific training task. The 2D finetuning objective is then defined as:

$$\mathcal{L}_{2\text{D}} = \frac{1}{K} \sum_{k=1}^K \ell(f(\mathcal{R}_{\text{spd}}^k, \mathcal{R}_{\text{edge}}^k, \mathcal{V}^k), \mathbf{y}_{2\text{D}}^k) \quad (12)$$

When it comes to scenarios where 3D information is obtained, we propose to incorporate both 2D and 3D information as model input, as generating 2D molecular graphs from 3D conformations is free and can bring in useful information from 2D perspective. The multimodal input is injected into the self-attention module that captures pair-wise relations:

$$\text{Attention}(\mathbf{Q}, \mathbf{K}, \mathbf{V}) = \text{softmax} \left(\frac{\mathbf{Q}\mathbf{K}^\top}{\sqrt{d}} + \Psi_{\text{SPD}} + \Psi_{\text{Edge}} + \Psi_{\text{Distance}} \right) \mathbf{V} \quad (13)$$

$$\mathcal{L}_{3\text{D}} = \frac{1}{K} \sum_{k=1}^K \ell(f(\mathcal{R}_{\text{spd}}^k, \mathcal{R}_{\text{edge}}^k, \mathcal{R}_{\text{distance}}^k, \mathcal{V}^k), \mathbf{y}_{3\text{D}}^k) \quad (14)$$

This practice is unique in utilizing information from multiple modalities for a single-modality task, which is infeasible in previous 3D [74] or multimodal methods with separate models for different modalities [36, 53, 34]. Empirically, we find that the integration of 2D information helps improve performance. we hypothesize that: 1) 2D information, such as chemical bond and connectivity on a molecular graph, encodes domain experts’ prior knowledge and provides references to 3D structure; 2) 3D structures obtained from computational simulations like DFT [7] can suffer from inevitable approximation errors [39] which are avoided in our approach.

3.4 Theoretical Insights

In this section, we present a theoretical perspective from mutual information maximization for a better understanding of the ‘blend-then-predict’ process. We demonstrate that this approach unifies existing contrastive, generative (inter-modality prediction), and mask-then-predict (intra-modality prediction) objectives within a single objective formulation.

For simplicity, we consider two relations, denoted as $\mathcal{R}_{2\text{D}} = (a_{ij})_{n \times n}$ and $\mathcal{R}_{3\text{D}} = (b_{ij})_{n \times n}$. Their elements are randomly partitioned into two parts, represented as $\mathcal{R}_{2\text{D}} = [A_1, A_2]$, $\mathcal{R}_{3\text{D}} = [B_1, B_2]$, such that A_i shares identical elements indexes with B_i , $i \in \{1, 2\}$. The blended matrix is denoted as $\mathcal{R}_{2\text{D}\&3\text{D}} = [A_1, B_2]$.

Proposition 3.1 (Mutual information Maximization) *The training process with modality-blending maximizes the lower bound of the following mutual information: $\mathbb{E}_{\mathcal{S}} I(A_2; A_1, B_2) + I(B_1; A_1, B_2)$. The proof can be found in Appendix A.2.4.*

Proposition 3.2 (Mutual Information Decomposition) *The mutual information $I(A_2; A_1, B_2) + I(B_1; A_1, B_2)$ can be decomposed into two components below. The first one corresponds to the objectives of current **contrastive and generative** approaches. The second component, which is the primary focus of our research, represents the **mask-then-predict** objective (proof in Proposition A.1*

in Appendix):

$$\begin{aligned}
 I(A_2; A_1, B_2) + I(B_1; A_1, B_2) = & \frac{1}{2} \left[\underbrace{I(A_1; B_1) + I(A_2; B_2)}_{\text{contrastive and generative}} + \underbrace{I(A_1; B_1|B_2) + I(A_2; B_2|A_1)}_{\text{conditional contrastive and generative}} \right] \\
 & + \frac{1}{2} \left[\underbrace{I(A_1; A_2) + I(B_1; B_2)}_{\text{mask-then-predict}} + \underbrace{I(A_1; A_2|B_2) + I(B_1; B_2|A_1)}_{\text{multimodal mask-then-predict}} \right]
 \end{aligned} \tag{15}$$

The first part of Equation 15 corresponds to existing (conditional) contrastive and generative methods, which aim to maximize the mutual information between two corresponding parts (A_i with B_i , $i \in \{1, 2\}$) across two modalities (see Appendix A.2.1 and A.2.3 for the detailed proof). The second part represents the (multimodal) mask-then-predict objectives, focusing on maximizing the mutual information between the masked and the remaining parts within a single modality (refer to Appendix A.2.2 for details).

This decomposition illustrates that our objective unifies contrastive, generative (inter-modality prediction), and mask-then-predict (intra-modality prediction) approaches within a single cohesive *blend-then-predict* framework, from the perspective of mutual information maximization. Moreover, this approach fosters enhanced cross-modal interaction by introducing an innovative multimodal mask-then-predict target.

4 Experiments

4.1 Experimental Setup

Datasets. For pretraining, we use PCQM4Mv2 dataset from the OGB Large-Scale Challenge [27], which includes 3.37 million molecules with both 2D graphs and 3D geometric structures. To evaluate the versatility of *MoleBLEND*, we carry out extensive experiments on 24 molecular tasks with different data formats across three representative benchmarks: MoleculeNet [64] (2D, 11 tasks), QM9 quantum properties [47] (3D, 12 tasks), and PCQM4Mv2 humo-lumo gap (2D). Further details about these datasets can be found in the Appendix B.1.

Baselines. We follow [34] to choose the most representative 2D and 3D pretraining baselines: AttrMask [28], ContextPred [28], InfoGraph [54], MolCLR [63], GraphCL [70], as well as recently published method Mole-BERT [65] and GraphMAE [26] as 2D baselines. In addition, we adopt GraphMVP [36], 3D InfoMax [53] and MoleculeSDE [34] as multimodal baselines.

Backbone Model. Following [68, 39], we employ a 12-layer Transformer of hidden size 768, with 32 attention heads. For pretraining, we use AdamW optimizer and set (β_1, β_2) to (0.9, 0.999) and peak learning rate to 1e-5. Batch size is 4096. We pretrain the model for 1 million steps with initial 100k steps as warm-up, after which learning rate decreases to zero following a cosine decay schedule.

4.2 Evaluation on 2D Capability

We evaluate *MoleBLEND* on molecular tasks in 2D format over the MoleculeNet, one of the most widely used benchmarks for molecular property prediction, which covers molecular properties ranging from quantum mechanics and physical chemistry to biophysics and physiology. We use the scaffold split [64], and report the mean and standard deviation of the results of 3 random seeds.

Table 1 presents the ROC-AUC scores for all compared methods on eight classification tasks. Remarkably, *MoleBLEND* achieves state-of-the-art performance in 7 out of 8 tasks, with significant margins in some cases (e.g., 83.7 v.s. 79.7 on Bace). Note that all other multimodal methods (3D Infomax [53], GraphMVP [36], MoleculeSDE [34]) utilize two separate modality-specific models, and use contrastive learning as one of their objectives. In contrast, *MoleBLEND* models molecules in a *unified* manner with a *fine-grained* relation-level integration of 2D and 3D modalities, which demonstrates superior performance. *MoleBLEND* also outperforms all 2D baselines (upper section of the table), demonstrating that incorporating 3D information helps improve the prediction of molecular properties. Table 3 summarizes the performance of different methods on three regression tasks of MoleculeNet. In all these tasks, *MoleBLEND* achieves state-of-the-art performance, further substantiating the superiority of unified fine-grained molecular modeling.

Table 1: Results on molecular property classification tasks (with 2D topology only). We report ROC-AUC score (higher is better) under scaffold splitting.

Pre-training Methods	BBBP \uparrow	Tox21 \uparrow	ToxCast \uparrow	SIDER \uparrow	ClinTox \uparrow	MUV \uparrow	HIV \uparrow	Bace \uparrow	Avg \uparrow
AttrMask [28]	65.0 \pm 2.36	74.8 \pm 0.25	62.9 \pm 0.11	61.2 \pm 0.12	87.7 \pm 1.19	73.4 \pm 2.02	76.8 \pm 0.53	79.7 \pm 0.33	72.68
ContextPred [28]	65.7 \pm 0.62	74.2 \pm 0.06	62.5 \pm 0.31	62.2 \pm 0.59	77.2 \pm 0.88	75.3 \pm 1.57	77.1 \pm 0.86	76.0 \pm 2.08	71.28
GraphCL [70]	69.7 \pm 0.67	73.9 \pm 0.66	62.4 \pm 0.57	60.5 \pm 0.88	76.0 \pm 2.65	69.8 \pm 2.66	78.5 \pm 1.22	75.4 \pm 1.44	70.78
InfoGraph [54]	67.5 \pm 0.11	73.2 \pm 0.43	63.7 \pm 0.50	59.9 \pm 0.30	76.5 \pm 1.07	74.1 \pm 0.74	75.1 \pm 0.99	77.8 \pm 0.88	70.98
GROVER [49]	70.0 \pm 0.10	74.3 \pm 0.10	65.4 \pm 0.40	64.8 \pm 0.60	81.2 \pm 3.00	67.3 \pm 1.80	62.5 \pm 0.90	82.6 \pm 0.70	71.01
MolCLR [63]	66.6 \pm 1.89	73.0 \pm 0.16	62.9 \pm 0.38	57.5 \pm 1.77	86.1 \pm 0.95	72.5 \pm 2.38	76.2 \pm 1.51	71.5 \pm 3.17	70.79
GraphMAE [26]	72.0 \pm 0.60	75.5 \pm 0.60	64.1 \pm 0.30	60.3 \pm 1.10	82.3 \pm 1.20	76.3 \pm 2.40	77.2 \pm 1.00	83.1 \pm 0.90	73.85
Mole-BERT [65]	71.9 \pm 1.60	76.8 \pm 0.50	64.3 \pm 0.20	62.8 \pm 1.10	78.9 \pm 3.00	78.6 \pm 1.80	78.2 \pm 0.80	80.8 \pm 1.40	74.04
3D InfoMax [53]	69.1 \pm 1.07	74.5 \pm 0.74	64.4 \pm 0.88	60.6 \pm 0.78	79.9 \pm 3.49	74.4 \pm 2.45	76.1 \pm 1.33	79.7 \pm 1.54	72.34
GraphMVP [36]	68.5 \pm 0.20	74.5 \pm 0.40	62.7 \pm 0.10	62.3 \pm 1.60	79.0 \pm 2.50	75.0 \pm 1.40	74.8 \pm 1.40	76.8 \pm 1.10	71.69
MoleculeSDE [34]	71.8 \pm 0.76	76.8 \pm 0.34	65.0 \pm 0.26	60.8 \pm 0.39	87.0 \pm 0.53	80.9\pm0.37	78.8 \pm 0.92	79.5 \pm 2.17	75.07
<i>MoleBLEND</i>	73.0\pm0.81	77.8\pm0.89	66.1\pm0.03	64.9\pm0.35	87.6\pm0.75	77.2 \pm 2.38	79.0\pm0.89	83.7\pm1.46	76.16

4.3 Evaluation on 3D Capability

We use QM9 [47] dataset to evaluate the effectiveness of *MoleBLEND* in 3D scenarios. QM9 is a quantum chemistry benchmark with 134K small organic molecules. It contains 12 tasks, covering the energetic, electronic and thermodynamic properties of molecules. Following [56], we randomly split 10,000 and 10,831 molecules as validation and test, respectively, with the remaining molecules for finetuning the model. Results are presented in Table 2, evaluated on MAE metric where lower number indicates better performance. *MoleBLEND* achieves state-of-the-art performance among multimodal methods on 8 out of 12 tasks, some of them with a large margin (e.g., Gap, HOMO, LUMO), demonstrating the strong capability of our model for 3D tasks.

Table 3: Results on molecular property prediction regression tasks (with 2D topology only). We report RMSE (lower is better) for each task.

Pre-training Methods	ESOL \downarrow	FreeSolv \downarrow	Lipo \downarrow
AttrMask [28]	1.112 \pm 0.048	-	0.730 \pm 0.004
ContextPred [28]	1.196 \pm 0.037	-	0.702 \pm 0.020
GROVER _{base} [49]	0.983 \pm 0.090	2.176 \pm 0.052	0.817 \pm 0.008
MolCLR [63]	1.271 \pm 0.040	2.594 \pm 0.249	0.691 \pm 0.004
3D InfoMax [53]	0.894 \pm 0.028	2.337 \pm 0.227	0.695 \pm 0.012
GraphMVP [36]	1.029 \pm 0.033	-	0.681 \pm 0.010
<i>MoleBLEND</i>	0.831\pm0.026	1.910\pm0.163	0.638\pm0.004

4.4 Evaluation on Large-Scale Challenge

PCQM4Mv2 dataset from the OGB Large-Scale Challenge focuses on predicting the HOMO-LUMO energy gap. They advocate for predicting quantum chemical properties using solely 2D molecular graphs without 3D equilibrium structures, which is practically favorable as obtaining 3D equilibrium structures necessitates costly DFT-based geometry optimization. This also makes it suitable for evaluating our model in large-scale scenarios where only 2D information is available. As shown in

Table 2: Results on QM9 datasets. Mean Absolute Error (MAE, lower is better) is reported.

Pre-training Methods	Alpha \downarrow	Gap \downarrow	HOMO \downarrow	LUMO \downarrow	Mu \downarrow	Cv \downarrow	G298 \downarrow	H298 \downarrow	R2 \downarrow	U298 \downarrow	U0 \downarrow	Zpve \downarrow
Distance Prediction [35]	0.065	45.87	27.61	23.34	0.031	0.033	14.83	15.81	0.248	15.07	15.01	1.837
3D InfoGraph [54]	0.062	45.96	29.29	24.60	0.028	0.030	13.93	13.97	0.133	13.55	13.47	1.644
3D InfoMax [53]	0.057	42.09	25.90	21.60	0.028	0.030	13.73	13.62	0.141	13.81	13.30	1.670
GraphMVP [36]	0.056	41.99	25.75	21.58	0.027	0.029	13.43	13.31	0.136	13.03	13.07	1.609
MoleculeSDE [34]	0.054	41.77	25.74	21.41	0.026	0.028	13.07	12.05	0.151	12.54	12.04	1.587
<i>MoleBLEND</i>	0.060	34.75	21.47	19.23	0.037	0.031	12.44	11.97	0.417	12.02	11.82	1.580

Table 4: Ablation studies on pretraining objectives. The best and second best results are marked by **bold** and underlined.

Pre-training Methods	BBBP \uparrow	Tox21 \uparrow	ToxCast \uparrow	SIDER \uparrow	ClinTox \uparrow	MUV \uparrow	HIV \uparrow	Bace \uparrow	U298 \downarrow	U0 \downarrow
Noisy-Node	68.50	<u>76.25</u>	65.48	63.71	83.28	78.80	79.13	82.72	<u>14.31</u>	<u>13.80</u>
Blend-then-Predict	<u>71.59</u>	75.61	<u>65.93</u>	<u>64.58</u>	90.82	76.81	79.74	<u>83.53</u>	14.56	15.35
<i>MoleBLEND</i>	73.00	77.82	66.14	64.90	<u>87.62</u>	<u>77.23</u>	<u>79.01</u>	83.66	12.02	11.82

Table 5, *MoleBLEND* establishes new state-of-the-art performance on PCQM4Mv2 dataset. This result validates our model in handling real-world, large-scale scenarios.

4.5 Ablation Studies

Pretraining Objectives Table 4 studies the effect of different pretraining objectives: noisy-node, blend-then-predict, and *MoleBLEND* (blend-then-predict with noisy-node as regularization). We observe that on most tasks, combining blend-then-predict and noisy-node yields better representations. In 2D scenarios, we find that blend-then-predict outperforms noisy-node on 5 out of 8 tasks studied, demonstrating its strong ability to process 2D inputs with practical value. While on 3D tasks (U298 and U0), blend-then-predict typically performs worse than noisy-node. This is because noisy-node is a pure 3D denoising task, which makes it more suitable for 3D tasks. We also show in Appendix C.1 that 3D pretraining methods achieve much faster convergence on 3D tasks than methods that incorporate 2D information. However, incorporating blend-then-predict can bring further performance boost, demonstrating that blend-then-predict is orthogonal and complementary to other state-of-the-art uni-modal methods.

Table 5: Results on PCQM4Mv2 validation set in OGB Large-Scale Challenge.

Methods	Valid MAE
CoAtGIN [76]	0.0933
TokenGT [31]	0.0910
GRPE [43]	0.0890
Graphormer [68]	0.0864
GraphGPS [48]	0.0858
Transformer-M [39]	0.0787
<i>MoleBLEND</i>	0.0777

Finetuning Settings When 3D molecular information is provided, we propose to incorporate both 2D topological and 3D structural information into the model, as generating 2D molecular graphs from 3D conformations is computationally inexpensive. Table 6 demonstrates that the inclusion of 2D information leads to a noticeable improvement in performance. We hypothesize that this is due to the fact that 2D information encodes chemical bond and connectivity on a molecular graph, which is grounded in prior knowledge of domain experts and provides valuable references to 3D structure. Note that this practice is a unique advantage of *MoleBLEND*, as we pretrain with both 2D and 3D information blended as a single input into a unified model, which is not feasible in previous multimodal methods that utilize two distinct models for 2D and 3D modalities.

Table 6: Ablation studies on finetuning settings of 3D tasks.

Finetune Settings	Alpha \downarrow	HOMO \downarrow	Mu \downarrow
3D	0.066	23.62	0.042
3D + 2D	0.060	21.47	0.037

5 Conclusion

We propose *MoleBLEND*, a novel self-supervised learning method for unified molecular modeling that organically integrates 2D and 3D modalities in a fine-grained manner. By treating atom relations as the anchor, we blend different modalities into an integral input for pretraining, which overcomes the limitations of existing approaches that distinguish 2D and 3D modalities as independent signals. Extensive experimental results reveal that *MoleBLEND* achieves state-of-the-art performance on a wide range of 2D and 3D benchmarks, demonstrating the superiority of unified modeling and fine-grained alignment of different modalities.

References

- [1] Alexander A Alemi, Ian Fischer, Joshua V Dillon, and Kevin Murphy. Deep variational information bottleneck. *arXiv preprint arXiv:1612.00410*, 2016. 14
- [2] Sanjeev Arora, Hrishikesh Khandeparkar, Mikhail Khodak, Orestis Plevrakis, and Nikunj Saunshi. A theoretical analysis of contrastive unsupervised representation learning. *arXiv preprint arXiv:1902.09229*, 2019. 15
- [3] Simon Axelrod and Rafael Gomez-Bombarelli. Geom, energy-annotated molecular conformations for property prediction and molecular generation. *Scientific Data*, 9(1):185, 2022. 1
- [4] Jimmy Lei Ba, Jamie Ryan Kiros, and Geoffrey E Hinton. Layer normalization. *arXiv preprint arXiv:1607.06450*, 2016. 3
- [5] Hangbo Bao, Li Dong, Songhao Piao, and Furu Wei. Beit: BERT pre-training of image transformers. In *The Tenth International Conference on Learning Representations, ICLR 2022, Virtual Event, April 25-29, 2022*. OpenReview.net, 2022. 3
- [6] Tom B. Brown, Benjamin Mann, Nick Ryder, Melanie Subbiah, Jared Kaplan, Prafulla Dhariwal, Arvind Neelakantan, Pranav Shyam, Girish Sastry, Amanda Askell, Sandhini Agarwal, Ariel Herbert-Voss, Gretchen Krueger, Tom Henighan, Rewon Child, Aditya Ramesh, Daniel M. Ziegler, Jeffrey Wu, Clemens Winter, Christopher Hesse, Mark Chen, Eric Sigler, Mateusz Litwin, Scott Gray, Benjamin Chess, Jack Clark, Christopher Berner, Sam McCandlish, Alec Radford, Ilya Sutskever, and Dario Amodei. Language models are few-shot learners. In Hugo Larochelle, Marc’Aurelio Ranzato, Raia Hadsell, Maria-Florina Balcan, and Hsuan-Tien Lin, editors, *Advances in Neural Information Processing Systems 33: Annual Conference on Neural Information Processing Systems 2020, NeurIPS 2020, December 6-12, 2020, virtual*, 2020. 3
- [7] Kieron Burke. Perspective on density functional theory. *The Journal of chemical physics*, 136(15):150901, 2012. 6
- [8] Mathilde Caron, Ishan Misra, Julien Mairal, Priya Goyal, Piotr Bojanowski, and Armand Joulin. Unsupervised learning of visual features by contrasting cluster assignments. In Hugo Larochelle, Marc’Aurelio Ranzato, Raia Hadsell, Maria-Florina Balcan, and Hsuan-Tien Lin, editors, *Advances in Neural Information Processing Systems 33: Annual Conference on Neural Information Processing Systems 2020, NeurIPS 2020, December 6-12, 2020, virtual*, 2020. 3
- [9] Ting Chen, Simon Kornblith, Mohammad Norouzi, and Geoffrey Hinton. A simple framework for contrastive learning of visual representations. In *International conference on machine learning*, pages 1597–1607. PMLR, 2020. 3, 15
- [10] Xinlei Chen and Kaiming He. Exploring simple siamese representation learning. In *Proceedings of the IEEE/CVF conference on computer vision and pattern recognition*, pages 15750–15758, 2021. 3
- [11] Xinlei Chen, Saining Xie, and Kaiming He. An empirical study of training self-supervised vision transformers. In *Proceedings of the IEEE/CVF International Conference on Computer Vision*, pages 9640–9649, 2021. 2
- [12] Yen-Chun Chen, Linjie Li, Licheng Yu, Ahmed El Kholy, Faisal Ahmed, Zhe Gan, Yu Cheng, and Jingjing Liu. UNITER: universal image-text representation learning. In Andrea Vedaldi, Horst Bischof, Thomas Brox, and Jan-Michael Frahm, editors, *Computer Vision - ECCV 2020 - 16th European Conference, Glasgow, UK, August 23-28, 2020, Proceedings, Part XXX*, volume 12375 of *Lecture Notes in Computer Science*, pages 104–120. Springer, 2020. 3
- [13] Seyone Chithrananda, Gabriel Grand, and Bharath Ramsundar. Chemberta: Large-scale self-supervised pretraining for molecular property prediction. *CoRR*, abs/2010.09885, 2020. 1
- [14] Thomas M. Cover and Joy A. Thomas. *Elements of Information Theory*, page 23. Wiley Online Library, 2nd edition, 1991. 14
- [15] Jacob Devlin, Ming-Wei Chang, Kenton Lee, and Kristina Toutanova. BERT: pre-training of deep bidirectional transformers for language understanding. In Jill Burstein, Christy Doran, and Thamar Solorio, editors, *Proceedings of the 2019 Conference of the North American Chapter of the Association for Computational Linguistics: Human Language Technologies, NAACL-HLT 2019, Minneapolis, MN, USA, June 2-7, 2019, Volume 1 (Long and Short Papers)*, pages 4171–4186. Association for Computational Linguistics, 2019. 3
- [16] Jacob Devlin, Ming-Wei Chang, Kenton Lee, and Kristina Toutanova. Bert: Pre-training of deep bidirectional transformers for language understanding. *arXiv preprint arXiv:1810.04805*, 2018. 15
- [17] Li Dong, Nan Yang, Wenhui Wang, Furu Wei, Xiaodong Liu, Yu Wang, Jianfeng Gao, Ming Zhou, and Hsiao-Wuen Hon. Unified language model pre-training for natural language understanding and generation. In Hanna M. Wallach, Hugo Larochelle, Alina Beygelzimer, Florence d’Alché-Buc, Emily B. Fox, and Roman Garnett, editors, *Advances in Neural Information Processing Systems 32: Annual Conference on Neural Information Processing Systems 2019, NeurIPS 2019, December 8-14, 2019, Vancouver, BC, Canada*, pages 13042–13054, 2019. 3
- [18] Xiaomin Fang, Lihang Liu, Jieqiong Lei, Donglong He, Shanzhuo Zhang, Jingbo Zhou, Fan Wang, Hua Wu, and Haifeng Wang. Geometry-enhanced molecular representation learning for property prediction. *Nature Machine Intelligence*, 4(2):127–134, 2022. 1

- [19] Yuxin Fang, Wen Wang, Binhui Xie, Quan Sun, Ledell Wu, Xinggang Wang, Tiejun Huang, Xinlong Wang, and Yue Cao. Eva: Exploring the limits of masked visual representation learning at scale. *arXiv preprint arXiv:2211.07636*, 2022. 3
- [20] Jonathan Godwin, Michael Schaarschmidt, Alexander L. Gaunt, Alvaro Sanchez-Gonzalez, Yulia Rubanova, Petar Velickovic, James Kirkpatrick, and Peter W. Battaglia. Simple GNN regularisation for 3d molecular property prediction and beyond. In *The Tenth International Conference on Learning Representations, ICLR 2022, Virtual Event, April 25-29, 2022*. OpenReview.net, 2022. 6
- [21] Christoph Gorgulla, Andras Boeszoermyeni, Zi-Fu Wang, Patrick D Fischer, Paul W Coote, Krishna M Padmanabha Das, Yehor S Malets, Dmytro S Radchenko, Yurii S Moroz, David A Scott, et al. An open-source drug discovery platform enables ultra-large virtual screens. *Nature*, 580(7805):663–668, 2020. 1
- [22] Jean-Bastien Grill, Florian Strub, Florent Altché, Corentin Tallec, Pierre Richemond, Elena Buchatskaya, Carl Doersch, Bernardo Avila Pires, Zhaohan Guo, Mohammad Gheshlaghi Azar, et al. Bootstrap your own latent—a new approach to self-supervised learning. *Advances in neural information processing systems*, 33:21271–21284, 2020. 3
- [23] Kaiming He, Xinlei Chen, Saining Xie, Yanghao Li, Piotr Dollár, and Ross Girshick. Masked autoencoders are scalable vision learners. In *Proceedings of the IEEE/CVF Conference on Computer Vision and Pattern Recognition*, pages 16000–16009, 2022. 3
- [24] Kaiming He, Haoqi Fan, Yuxin Wu, Saining Xie, and Ross Girshick. Momentum contrast for unsupervised visual representation learning. In *Proceedings of the IEEE/CVF conference on computer vision and pattern recognition*, pages 9729–9738, 2020. 3
- [25] Kaiming He, Xiangyu Zhang, Shaoqing Ren, and Jian Sun. Deep residual learning for image recognition. In *Proceedings of the IEEE conference on computer vision and pattern recognition*, pages 770–778, 2016. 3
- [26] Zhenyu Hou, Xiao Liu, Yukuo Cen, Yuxiao Dong, Hongxia Yang, Chunjie Wang, and Jie Tang. Graphmae: Self-supervised masked graph autoencoders. In Aidong Zhang and Huzefa Rangwala, editors, *KDD '22: The 28th ACM SIGKDD Conference on Knowledge Discovery and Data Mining, Washington, DC, USA, August 14 - 18, 2022*, pages 594–604. ACM, 2022. 7, 8
- [27] Weihua Hu, Matthias Fey, Hongyu Ren, Maho Nakata, Yuxiao Dong, and Jure Leskovec. OGB-LSC: A large-scale challenge for machine learning on graphs. In Joaquin Vanschoren and Sai-Kit Yeung, editors, *Proceedings of the Neural Information Processing Systems Track on Datasets and Benchmarks 1, NeurIPS Datasets and Benchmarks 2021, December 2021, virtual*, 2021. 7
- [28] Weihua Hu, Bowen Liu, Joseph Gomes, Marinka Zitnik, Percy Liang, Vijay S. Pande, and Jure Leskovec. Strategies for pre-training graph neural networks. In *8th International Conference on Learning Representations, ICLR 2020, Addis Ababa, Ethiopia, April 26-30, 2020*. OpenReview.net, 2020. 1, 7, 8
- [29] Rui Jiao, Jiaqi Han, Wenbing Huang, Yu Rong, and Yang Liu. Energy-motivated equivariant pretraining for 3d molecular graphs. *arXiv preprint arXiv:2207.08824*, 2022. 1
- [30] Guolin Ke, Di He, and Tie-Yan Liu. Rethinking positional encoding in language pre-training. In *9th International Conference on Learning Representations, ICLR 2021, Virtual Event, Austria, May 3-7, 2021*. OpenReview.net, 2021. 3
- [31] Jinwoo Kim, Dat Nguyen, Seonwoo Min, Sungjun Cho, Moontae Lee, Honglak Lee, and Seunghoon Hong. Pure transformers are powerful graph learners. In *NeurIPS*, 2022. 9
- [32] Lingpeng Kong, Cyprien de Masson d’Autume, Wang Ling, Lei Yu, Zihang Dai, and Dani Yogatama. A mutual information maximization perspective of language representation learning. *arXiv preprint arXiv:1910.08350*, 2019. 15
- [33] Ralph Linsker. An application of the principle of maximum information preservation to linear systems. *Advances in neural information processing systems*, 1, 1988. 14
- [34] Shengchao Liu, Weitao Du, Zhiming Ma, Hongyu Guo, and Jian Tang. A group symmetric stochastic differential equation model for molecule multi-modal pretraining. In *International Conference on Learning Representations*, 2023. 1, 2, 3, 6, 7, 8
- [35] Shengchao Liu, Hongyu Guo, and Jian Tang. Molecular geometry pretraining with se (3)-invariant denoising distance matching. *arXiv preprint arXiv:2206.13602*, 2022. 1, 8
- [36] Shengchao Liu, Hanchen Wang, Weiyang Liu, Joan Lasenby, Hongyu Guo, and Jian Tang. Pre-training molecular graph representation with 3d geometry. In *International Conference on Learning Representations*, 2022. 1, 2, 3, 6, 7, 8, 15
- [37] Yinhan Liu, Myle Ott, Naman Goyal, Jingfei Du, Mandar Joshi, Danqi Chen, Omer Levy, Mike Lewis, Luke Zettlemoyer, and Veselin Stoyanov. Roberta: A robustly optimized BERT pretraining approach. *CoRR*, abs/1907.11692, 2019. 3
- [38] Yi Liu, Limei Wang, Meng Liu, Xuan Zhang, Bora Oztekin, and Shuiwang Ji. Spherical message passing for 3d graph networks. *CoRR*, abs/2102.05013, 2021. 2
- [39] Shengjie Luo, Tianlang Chen, Yixian Xu, Shuxin Zheng, Tie-Yan Liu, Liwei Wang, and Di He. One transformer can understand both 2d & 3d molecular data. *arXiv preprint arXiv:2210.01765*, 2022. 1, 2, 3, 5, 6, 7, 9

- [40] David McAllester and Karl Stratos. Formal limitations on the measurement of mutual information. In *International Conference on Artificial Intelligence and Statistics*, pages 875–884. PMLR, 2020. 14
- [41] Yuyan Ni, Yanyan Lan, Ao Liu, and Zhiming Ma. Elastic information bottleneck. *Mathematics*, 10(18):3352, 2022. 14
- [42] Aaron van den Oord, Yazhe Li, and Oriol Vinyals. Representation learning with contrastive predictive coding. *arXiv preprint arXiv:1807.03748*, 2018. 15
- [43] Wonpyo Park, Woong-Gi Chang, Donggeon Lee, Juntae Kim, et al. Grpe: Relative positional encoding for graph transformer. In *ICLR2022 Machine Learning for Drug Discovery*, 2022. 9
- [44] Ben Poole, Sherjil Ozair, Aaron Van Den Oord, Alex Alemi, and George Tucker. On variational bounds of mutual information. In *International Conference on Machine Learning*, pages 5171–5180. PMLR, 2019. 14
- [45] Alec Radford, Jong Wook Kim, Chris Hallacy, Aditya Ramesh, Gabriel Goh, Sandhini Agarwal, Girish Sastry, Amanda Askell, Pamela Mishkin, Jack Clark, Gretchen Krueger, and Ilya Sutskever. Learning transferable visual models from natural language supervision. In Marina Meila and Tong Zhang, editors, *Proceedings of the 38th International Conference on Machine Learning, ICML 2021, 18-24 July 2021, Virtual Event*, volume 139 of *Proceedings of Machine Learning Research*, pages 8748–8763. PMLR, 2021. 2, 3
- [46] Colin Raffel, Noam Shazeer, Adam Roberts, Katherine Lee, Sharan Narang, Michael Matena, Yanqi Zhou, Wei Li, and Peter J Liu. Exploring the limits of transfer learning with a unified text-to-text transformer. *The Journal of Machine Learning Research*, 21(1):5485–5551, 2020. 3, 5
- [47] Raghunathan Ramakrishnan, Pavlo O Dral, Matthias Rupp, and O Anatole Von Lilienfeld. Quantum chemistry structures and properties of 134 kilo molecules. *Scientific data*, 1(1):1–7, 2014. 7, 8, 17
- [48] Ladislav Rampásek, Michael Galkin, Vijay Prakash Dwivedi, Anh Tuan Luu, Guy Wolf, and Dominique Beaini. Recipe for a general, powerful, scalable graph transformer. In *NeurIPS*, 2022. 9
- [49] Yu Rong, Yatao Bian, Tingyang Xu, Weiyang Xie, Ying Wei, Wenbing Huang, and Junzhou Huang. Self-supervised graph transformer on large-scale molecular data. *Advances in Neural Information Processing Systems*, 33:12559–12571, 2020. 1, 8
- [50] Bernhard Schölkopf, Kah Kay Sung, Christopher J. C. Burges, Federico Girosi, Partha Niyogi, Tomaso A. Poggio, and Vladimir Vapnik. Comparing support vector machines with gaussian kernels to radial basis function classifiers. *IEEE Trans. Signal Process.*, 45(11):2758–2765, 1997. 5
- [51] Kristof Schütt, Pieter-Jan Kindermans, Huziel Enoc Saucedo Felix, Stefan Chmiela, Alexandre Tkatchenko, and Klaus-Robert Müller. Schnet: A continuous-filter convolutional neural network for modeling quantum interactions. In Isabelle Guyon, Ulrike von Luxburg, Samy Bengio, Hanna M. Wallach, Rob Fergus, S. V. N. Vishwanathan, and Roman Garnett, editors, *Advances in Neural Information Processing Systems 30: Annual Conference on Neural Information Processing Systems 2017, December 4-9, 2017, Long Beach, CA, USA*, pages 991–1001, 2017. 2
- [52] Peter Shaw, Jakob Uszkoreit, and Ashish Vaswani. Self-attention with relative position representations. In Marilyn A. Walker, Heng Ji, and Amanda Stent, editors, *Proceedings of the 2018 Conference of the North American Chapter of the Association for Computational Linguistics: Human Language Technologies, NAACL-HLT, New Orleans, Louisiana, USA, June 1-6, 2018, Volume 2 (Short Papers)*, pages 464–468. Association for Computational Linguistics, 2018. 3
- [53] Hannes Stärk, Dominique Beaini, Gabriele Corso, Prudencio Tossou, Christian Dallago, Stephan Günemann, and Pietro Liò. 3d infomax improves gnns for molecular property prediction. In *International Conference on Machine Learning*, pages 20479–20502. PMLR, 2022. 1, 2, 3, 6, 7, 8
- [54] Fan-Yun Sun, Jordan Hoffmann, Vikas Verma, and Jian Tang. Infograph: Unsupervised and semi-supervised graph-level representation learning via mutual information maximization. In *8th International Conference on Learning Representations, ICLR 2020, Addis Ababa, Ethiopia, April 26-30, 2020*. OpenReview.net, 2020. 1, 7, 8
- [55] Quan Sun, Qiyang Yu, Yufeng Cui, Fan Zhang, Xiaosong Zhang, Yueze Wang, Hongcheng Gao, Jingjing Liu, Tiejun Huang, and Xinlong Wang. Generative pretraining in multimodality. 2023. 3
- [56] Philipp Thölke and Gianni De Fabritiis. Equivariant transformers for neural network based molecular potentials. In *The Tenth International Conference on Learning Representations, ICLR 2022, Virtual Event, April 25-29, 2022*. OpenReview.net, 2022. 8
- [57] Naftali Tishby, Fernando C Pereira, and William Bialek. The information bottleneck method. *arXiv preprint physics/0004057*, 2000. 14
- [58] Ashish Vaswani, Noam Shazeer, Niki Parmar, Jakob Uszkoreit, Llion Jones, Aidan N Gomez, Łukasz Kaiser, and Illia Polosukhin. Attention is all you need. *Advances in neural information processing systems*, 30, 2017. 3
- [59] Pascal Vincent, Hugo Larochelle, Yoshua Bengio, and Pierre-Antoine Manzagol. Extracting and composing robust features with denoising autoencoders. In *Proceedings of the 25th international conference on Machine learning*, pages 1096–1103, 2008. 3
- [60] Sheng Wang, Yuzhi Guo, Yuhong Wang, Hongmao Sun, and Junzhou Huang. SMILES-BERT: large scale unsupervised pre-training for molecular property prediction. In Xinghua Mindy Shi, Michael

- Buck, Jian Ma, and Pierangelo Veltri, editors, *Proceedings of the 10th ACM International Conference on Bioinformatics, Computational Biology and Health Informatics, BCB 2019, Niagara Falls, NY, USA, September 7-10, 2019*, pages 429–436. ACM, 2019. 1
- [61] Wenhui Wang, Hangbo Bao, Li Dong, Johan Bjorck, Zhiliang Peng, Qiang Liu, Kriti Aggarwal, Owais Khan Mohammed, Saksham Singhal, Subhojit Som, and Furu Wei. Image as a foreign language: Beit pretraining for all vision and vision-language tasks. *CoRR*, abs/2208.10442, 2022. 3
- [62] Yuyang Wang, Rishikesh Magar, Chen Liang, and Amir Barati Farimani. Improving molecular contrastive learning via faulty negative mitigation and decomposed fragment contrast. *J. Chem. Inf. Model.*, 62(11):2713–2725, 2022. 1
- [63] Yuyang Wang, Jianren Wang, Zhonglin Cao, and Amir Barati Farimani. Molecular contrastive learning of representations via graph neural networks. *Nat. Mach. Intell.*, 4(3):279–287, 2022. 1, 7, 8
- [64] Zhenqin Wu, Bharath Ramsundar, Evan N. Feinberg, Joseph Gomes, Caleb Geniesse, Aneesh S. Pappu, Karl Leswing, and Vijay S. Pande. Moleculenet: A benchmark for molecular machine learning. *CoRR*, abs/1703.00564, 2017. 7, 16
- [65] Jun Xia, Chengshuai Zhao, Bozhen Hu, Zhangyang Gao, Cheng Tan, Yue Liu, Siyuan Li, and Stan Z Li. Mole-bert: Rethinking pre-training graph neural networks for molecules. 2023. 1, 7, 8
- [66] Zhenda Xie, Zigang Geng, Jingcheng Hu, Zheng Zhang, Han Hu, and Yue Cao. Revealing the dark secrets of masked image modeling. *arXiv preprint arXiv:2205.13543*, 2022. 2
- [67] Zhenda Xie, Zheng Zhang, Yue Cao, Yutong Lin, Jianmin Bao, Zhuliang Yao, Qi Dai, and Han Hu. Simmim: A simple framework for masked image modeling. In *Proceedings of the IEEE/CVF Conference on Computer Vision and Pattern Recognition*, pages 9653–9663, 2022. 3
- [68] Chengxuan Ying, Tianle Cai, Shengjie Luo, Shuxin Zheng, Guolin Ke, Di He, Yanming Shen, and Tie-Yan Liu. Do transformers really perform badly for graph representation? *Advances in Neural Information Processing Systems*, 34:28877–28888, 2021. 3, 7, 9
- [69] Yuning You, Tianlong Chen, Yang Shen, and Zhangyang Wang. Graph contrastive learning automated. In Marina Meila and Tong Zhang, editors, *Proceedings of the 38th International Conference on Machine Learning, ICML 2021, 18-24 July 2021, Virtual Event*, volume 139 of *Proceedings of Machine Learning Research*, pages 12121–12132. PMLR, 2021. 1
- [70] Yuning You, Tianlong Chen, Yongduo Sui, Ting Chen, Zhangyang Wang, and Yang Shen. Graph contrastive learning with augmentations. In Hugo Larochelle, Marc’Aurelio Ranzato, Raia Hadsell, Maria-Florina Balcan, and Hsuan-Tien Lin, editors, *Advances in Neural Information Processing Systems 33: Annual Conference on Neural Information Processing Systems 2020, NeurIPS 2020, December 6-12, 2020, virtual*, 2020. 1, 7, 8
- [71] Qiying Yu, Yang Liu, Yimu Wang, Ke Xu, and Jingjing Liu. Multimodal federated learning via contrastive representation ensemble. *CoRR*, abs/2302.08888, 2023. 3
- [72] Qiying Yu, Jieming Lou, Xianyuan Zhan, Qizhang Li, Wangmeng Zuo, Yang Liu, and Jingjing Liu. Adversarial contrastive learning via asymmetric infonce. In *Computer Vision—ECCV 2022: 17th European Conference, Tel Aviv, Israel, October 23–27, 2022, Proceedings, Part V*, pages 53–69. Springer, 2022. 3
- [73] Mert Yuksekgonul, Federico Bianchi, Pratyusha Kalluri, Dan Jurafsky, and James Zou. When and why vision-language models behave like bag-of-words models, and what to do about it? *arXiv preprint arXiv:2210.01936*, 2022. 2
- [74] Sheheryar Zaidi, Michael Schaarschmidt, James Martens, Hyunjik Kim, Yee Whye Teh, Alvaro Sanchez-Gonzalez, Peter Battaglia, Razvan Pascanu, and Jonathan Godwin. Pre-training via denoising for molecular property prediction. *arXiv preprint arXiv:2206.00133*, 2022. 1, 6
- [75] Jure Zbontar, Li Jing, Ishan Misra, Yann LeCun, and Stéphane Deny. Barlow twins: Self-supervised learning via redundancy reduction. In Marina Meila and Tong Zhang, editors, *Proceedings of the 38th International Conference on Machine Learning, ICML 2021, 18-24 July 2021, Virtual Event*, volume 139 of *Proceedings of Machine Learning Research*, pages 12310–12320. PMLR, 2021. 3
- [76] Xuan Zhang, Cheng Chen, Zhaoxu Meng, Zhenghe Yang, Haitao Jiang, and Xuefeng Cui. Coatgin: Marrying convolution and attention for graph-based molecule property prediction. In Donald A. Adjeroh, Qi Long, Xinghua Mindy Shi, Fei Guo, Xiaohua Hu, Srinivas Aluru, Giri Narasimhan, Jianxin Wang, Mingon Kang, Ananda Mondal, and Jin Liu, editors, *IEEE International Conference on Bioinformatics and Biomedicine, BIBM 2022, Las Vegas, NV, USA, December 6-8, 2022*, pages 374–379. IEEE, 2022. 9
- [77] Zaixi Zhang, Qi Liu, Hao Wang, Chengqiang Lu, and Chee-Kong Lee. Motif-based graph self-supervised learning for molecular property prediction. In Marc’Aurelio Ranzato, Alina Beygelzimer, Yann N. Dauphin, Percy Liang, and Jennifer Wortman Vaughan, editors, *Advances in Neural Information Processing Systems 34: Annual Conference on Neural Information Processing Systems 2021, NeurIPS 2021, December 6-14, 2021, virtual*, pages 15870–15882, 2021. 1
- [78] Gengmo Zhou, Zhifeng Gao, Qiankun Ding, Hang Zheng, Hongteng Xu, Zhewei Wei, Linfeng Zhang, and Guolin Ke. Uni-mol: A universal 3d molecular representation learning framework. 2023. 1, 5
- [79] Jinhua Zhu, Yingce Xia, Lijun Wu, Shufang Xie, Tao Qin, Wengang Zhou, Houqiang Li, and Tie-Yan Liu. Unified 2d and 3d pre-training of molecular representations. *arXiv preprint arXiv:2207.08806*, 2022. 1, 3

A Theoretical analysis

In the following sections, we follow common notations[14], using uppercase letters to represent random variables and lowercase letters to represent samples of the random variables.

A.1 Missing Proofs

Lemma A.1 (Chain rule of mutual information[14])

$$I(X_1, X_2; Y) = I(X_1; Y) + I(X_2; Y|X_1) \quad (16)$$

Proof

$$\begin{aligned} I(X_1; Y) + I(X_2; Y|X_1) &= E_{p(x_1, y)} \left[\log \frac{p(x_1, y)}{p(x_1)p(y)} \right] + E_{p(x_1, x_2, y)} \left[\log \frac{p(x_2, y|x_1)}{p(x_2|x_1)p(y|x_1)} \right] \\ &= E_{p(x_1, x_2, y)} \left[\log \frac{p(x_1, y)}{p(x_1)p(y)} \frac{p(x_2, y|x_1)}{p(x_2|x_1)p(y|x_1)} \right] \\ &= E_{p(x_1, x_2, y)} \left[\log \frac{p(x_1, y)p(x_2, y, x_1)}{p(y)p(x_2, x_1)p(y, x_1)} \right] \\ &= E_{p(x_1, x_2, y)} \left[\log \frac{p(x_2, y, x_1)}{p(y)p(x_2, x_1)} \right] = I(X_1, X_2; Y) \end{aligned} \quad (17)$$

Proposition A.1 (Mutual Information Decomposition) *The blend-and-predict method is maximizing the lower bound of the mutual information target below, which can be further divided into two parts.*

$$\begin{aligned} &I(A_2; A_1, B_2) + I(B_1; A_1, B_2) \\ &= \frac{1}{2} [I(A_1; B_1) + I(A_2; B_2) + I(A_1; B_1|B_2) + I(A_2; B_2|A_1)] + \\ &\quad \frac{1}{2} [I(A_1; A_2) + I(B_1; B_2) + I(A_1; A_2|B_2) + I(B_1; B_2|A_1)] \end{aligned} \quad (18)$$

Proof Firstly, we provide the decomposition of first term in (18), i.e. $I(A_2; A_1, B_2)$. By using Lemma A.1 and letting $X_1 = A_1$, $X_2 = B_2$ and $Y = A_2$, we have

$$I(A_2; A_1, B_2) = I(A_1; A_2) + I(A_2; B_2|A_1). \quad (19)$$

Again use Lemma A.1 and let $X_1 = B_2$, $X_2 = A_1$ and $Y = A_2$, then we have

$$I(A_2; A_1, B_2) = I(B_2; A_2) + I(A_2; A_1|B_2). \quad (20)$$

From (19) and (20), we have

$$I(A_2; A_1, B_2) = \frac{1}{2} [I(A_1; A_2) + I(A_2; B_2|A_1) + I(B_2; A_2) + I(A_2; A_1|B_2)]. \quad (21)$$

Similarly, we apply Lemma A.1 to decompose the second term in (18).

$$I(B_1; A_1, B_2) = \frac{1}{2} [I(B_1; A_1) + I(B_2; B_2|A_1) + I(B_1; B_2) + I(B_1; A_1|B_2)]. \quad (22)$$

End of proof.

A.2 Mutual Information and Self-supervised Learning Tasks

A core objective of machine learning is to learn effective data representations. Many methods attempt to achieve this goal through maximizing mutual information (MI), e.g. InfoMax principle [33] and information bottleneck principle [57]. Unfortunately, estimating MI is intractable in general [40]. Therefore, many works resort to optimize the upper or lower bound of MI [1, 44, 41]

In the field of self-supervised learning (SSL), there are two widely used methods for acquiring meaningful representations: contrastive methods and predictive (generative) methods. Recently, it has been discovered that these two methods are closely linked to the maximization of lower-bound mutual information (MI) targets. A summary of these relationships is presented below.

A.2.1 Contrastive Objective

Contrastive learning (CL) [9] learn representations that are similar between positive pairs while distinct between negative pairs. From the perspective of mutual information maximization, CL actually maximizes the mutual information between the representations of positive pairs. The InfoNCE loss [42, 32] is given by:

$$\mathcal{L}_{\text{InfoNCE}} = -E_{p(x,y)} \left[\log \frac{f(x,y)}{\sum_{\tilde{y} \in \tilde{\mathcal{Y}}} f(x,\tilde{y})} \right] \quad (23)$$

where (x, y) is a positive pair, $\tilde{\mathcal{Y}}$ is the sample set containing the positive sample y and $|\tilde{\mathcal{Y}}| - 1$ negative samples of x , $f(\cdot, \cdot)$ characterizes the similarity between the two input variables. [42] proved that minimizing the InfoNCE loss is maximizing a lower bound of the following mutual information:

$$I(X; Y) \geq \log |\tilde{\mathcal{Y}}| - \mathcal{L}_{\text{InfoNCE}}. \quad (24)$$

Denote v_1 and v_2 as two views of the input and h_θ is the representation function. Define $x = h_\theta(v_1)$ and $y = h_\theta(v_2)$ as representations of the two views and the similarity function $f(x, y) = \exp(x^\top y)$, contrastive learning is optimizing the following InfoNCE loss [2]

$$\mathcal{L}_{\text{CL}} = -E_{p(v_1, v_2^+, v_2^-)} \left[\log \frac{\exp(h_\theta(v_1)^\top h_\theta(v_2^+))}{\exp(h_\theta(v_1)^\top h_\theta(v_2^+)) + \sum_{v_2^-} \exp(h_\theta(v_1)^\top h_\theta(v_2^-))} \right], \quad (25)$$

where v_2^+ is the positive sample, v_2^- is negative samples. Accordingly, minimizing the CL loss is maximizing the lower bound of $I(h_\theta(v_1), h_\theta(v_2))$ w.r.t. the representation function.

A.2.2 Predictive Objective (Mask-then-Predict)

The mask-then-predict task [16] are revealed to maximize the mutual information between the representations of the context and the masked tokens [32]. A lower bound of this MI can be derived in the form of a predictive loss:

$$\begin{aligned} I(X; Y) &= H(Y) - H(Y|X) \geq -H(Y|X) \\ &= E_{p(x,y)} [\log p(y|x)] \geq E_{p(x,y)} [\log q(y|x)]. \end{aligned} \quad (26)$$

The last inequation holds by applying the Jensen inequation $E_{p(x,y)} [\log \frac{q(y|x)}{p(y|x)}] \leq \log E_{p(x,y)} [\frac{q(y|x)}{p(y|x)}] = 0$.

Denote $x = h_\theta(c)$ and $y = h_\theta(m)$ as representations of the context c and the masked token m to be predicted. q_ϕ is the predictive model. This predictive objective $E_{p(c,m)} [\log q_\phi(h_\theta(m)|h_\theta(c))]$ corresponds to the training objective of a mask-then-predict task. Therefore, according to (26), mask-then-predict task maximizes the lower bound of the MI between representations of the context and the masked tokens, i.e.

$$I(h_\theta(C), h_\theta(M)) \geq E_{p(c,m)} [\log q_\phi(h_\theta(m)|h_\theta(c))]. \quad (27)$$

A.2.3 Generative Objective

[36] conducts cross-modal pretraining by generating representations of one modality from the other. Utilizing (26) and the symmetry of mutual information, we can derive a lower bound of MI in the form of a mutual generative loss:

$$I(X; Y) \geq \frac{1}{2} E_{p(x,y)} [\log q(y|x) + \log q(x|y)]. \quad (28)$$

Denote v_1 and v_2 as two views of the input. h_θ is the representation function and q_ϕ is the predictive model. In (28), let $x = h_\theta(v_1)$ and $y = h_\theta(v_2)$, then we can derive that learning to generate the representation of one view from the other corresponds to maximize the lower bound of mutual information between the representations of the two views:

$$I(h_\theta(V_1), h_\theta(V_2)) \geq \frac{1}{2} E_{p(v_1, v_2)} [\log q_{\phi_1}(h_\theta(v_1)|h_\theta(v_2)) + \log q_{\phi_2}(h_\theta(v_2)|h_\theta(v_1))]. \quad (29)$$

A.2.4 Modality Blending

We next present an theoretical understanding of multimodal blend-then-predict. For simplicity, we consider two relations, denoted as $\mathcal{R}_{2D} = (a_{ij})_{n \times n}$ and $\mathcal{R}_{3D} = (b_{ij})_{n \times n}$. Their elements are randomly partitioned into two parts by random partition variable S , represented as $\mathcal{R}_{2D} = [A_1, A_2]$, $\mathcal{R}_{3D} = [B_1, B_2]$, such that A_i shares identical elements indexes with B_i , $i \in \{1, 2\}$. The blended matrix is denoted as $\mathcal{R}_{2D\&3D} = [A_1, B_2]$. Our objective is to predict the two full modalities from the blended relations:

$$\max_{\theta, \phi_1, \phi_2} E_S E_{p(a_1, a_2, b_1, b_2)} [\log q_{\phi_1}(h_{\theta}(a_2)|h_{\theta}(a_1), h_{\theta}(b_2)) + \log q_{\phi_2}(h_{\theta}(b_1)|h_{\theta}(a_1), h_{\theta}(b_2))], \quad (30)$$

where h_{θ} is the representation extractor, q_{ϕ_1} and q_{ϕ_2} are predictive head that recovers \mathcal{R}_{2D} and \mathcal{R}_{3D} . Utilizing the result from (27), the blend-then-predict objective aims to maximize the lower bound of mutual information presented below:

$$E_S I(h_{\theta}(A_2); h_{\theta}(A_1), h_{\theta}(B_2)) + I(h_{\theta}(B_1); h_{\theta}(A_1), h_{\theta}(B_2)). \quad (31)$$

From the mutual information decomposition in Proposition A.1, the objective in (31) can be divided into two parts.

$$\begin{aligned} & E_S \left\{ \frac{1}{2} \underbrace{[I(A_1; B_1) + I(A_2; B_2)]}_{\text{contrastive and generative}} + \underbrace{[I(A_1; B_1|B_2) + I(A_2; B_2|A_1)]}_{\text{conditional contrastive and generative}} \right\} \\ & + \frac{1}{2} \left\{ \underbrace{[I(A_1; A_2) + I(B_1; B_2)]}_{\text{mask-then-predict}} + \underbrace{[I(A_1; A_2|B_2) + I(B_1; B_2|A_1)]}_{\text{multimodal mask-then-predict}} \right\} \end{aligned} \quad (32)$$

The first part of Equation 32 corresponds to existing (conditional) contrastive and generative methods, which aim to maximize the mutual information between two corresponding parts (A_i with B_i , $i \in \{1, 2\}$) across two modalities. The second part represents the (multimodal) mask-then-predict objectives, focusing on maximizing the mutual information between the masked and the remaining parts within a single modality.

This decomposition demonstrates that our objective unifies contrastive, generative (inter-modality prediction), and mask-then-predict (intra-modality prediction) approaches within a single cohesive *blend-then-predict* framework, from the perspective of mutual information maximization. Moreover, this approach fosters enhanced cross-modal interaction by introducing an innovative multimodal mask-then-predict target.

B Experimental Details

B.1 Datasets Details

MoleculeNet [64] 11 datasets are used to evaluate model performance on 2D tasks:

- **BBBP**: The blood-brain barrier penetration dataset, aims at modeling and predicting the barrier permeability.
- **Tox21**: This dataset (“Toxicology in the 21st Century”) contains qualitative toxicity measurements for 8014 compounds on 12 different targets, including nuclear receptors and stress response pathways.
- **ToxCast**: ToxCast is another data collection providing toxicology data for a large library of compounds based on in vitro high-throughput screening, including qualitative results of over 600 experiments on 8615 compounds.
- **SIDER**: The Side Effect Resource (SIDER) is a database of marketed drugs and adverse drug reactions (ADR), grouped into 27 system organ classes.
- **ClinTox**: The ClinTox dataset compares drugs approved by the FDA and drugs that have failed clinical trials for toxicity reasons. The dataset includes two classification tasks for 1491 drug compounds with known chemical structures: (1) clinical trial toxicity (or absence of toxicity) and (2) FDA approval status.

Table 7: Hyperparameters setup for pretraining.

Hyperparameter	Value
Max learning rate	1e-5
Min learning rate	0
Learning rate schedule	cosine
Optimizer	Adam
Adam betas	(0.9, 0.999)
Batch size	4096
Training steps	1,000,000
Warmup steps	100,000
Weight Decay	0.0
num. of layers	12
num. of attention heads	32
embedding dim	768
num. of 3D Gaussian kernel	128

Table 8: Search space for MoleculeNet tasks. Small datasets: BBBP, BACE, ClinTox, Tox21, Toxcast, SIDER, ESOL FreeSolv, Lipo. Large datasets: MUV.

Hyperparameter	Small	Large	HIV
Learning rate	[1e-6, 1e-4]	[1e-6, 1e-4]	[1e6, 1e-4]
Batch size	{32,64,128,256}	{128,256}	{128,256}
Epochs	{40, 60, 80, 100}	{20, 40}	{2, 5, 10}
Weight Decay	[1e-7, 1e-3]	[1e-7, 1e-3]	[1e-7, 1e-3]

- MUV: The Maximum Unbiased Validation (MUV) group is another benchmark dataset selected from PubChem BioAssay by applying a refined nearest neighbor analysis, containing 17 challenging tasks for around 90,000 compounds and is specifically designed for validation of virtual screening techniques.
- HIV: The HIV dataset was introduced by the Drug Therapeutics Program (DTP) AIDS Antiviral Screen, which tested the ability to inhibit HIV replication for over 40,000 compounds.
- BACE: The BACE dataset provides qualitative binding results for a set of inhibitors of human β -secretase 1. 1522 compounds with their 2D structures and binary labels are collected, built as a classification task.
- ESOL: ESOL is a small dataset consisting of water solubility data for 1128 compounds.
- FreeSolv: The Free Solvation Database provides experimental and calculated hydration free energy of small molecules in water.
- Lipo: Lipophilicity is an important feature of drug molecules that affects both membrane permeability and solubility. This dataset provides experimental results of octanol/water distribution coefficient (logD at pH 7.4) of 4200 compounds.

QM9 [47] QM9 is a quantum chemistry benchmark consisting of 134k stable small organic molecules, corresponding to the subset of all 133,885 species out of the GDB-17 chemical universe of 166 billion organic molecules. The molecules in QM9 contains up to 9 heavy atoms. Each molecule is associated with 12 targets covering its geometric, energetic, electronic, and thermodynamic properties, which are calculated by density functional theory (DFT).

B.2 Hyperparameters

Hyperparameters for pretraining and finetuning on MoleculeNet and QM9 benchmarks are presented in Table 7, Table 8 and Table 9, respectively.

Table 9: Hyperparameters for QM9 finetuning.

Hyperparameter	QM9
Peak Learning rate	1e-4
End Learning rate	1e-9
Batch size	128
Warmup Steps	60,000
Max Steps	600,000
Weight Decay	0.0

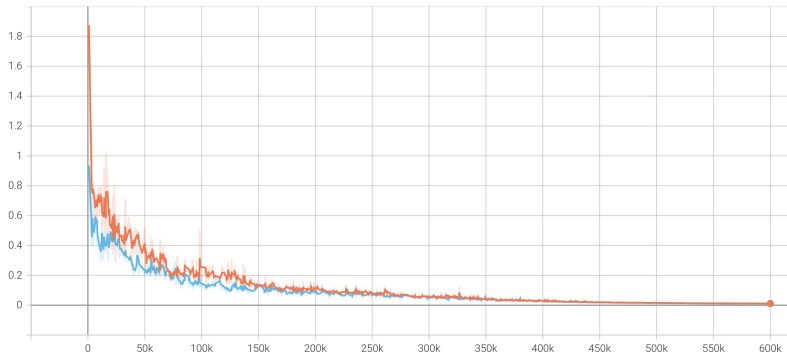


Figure 3: Training curves of Noisy-Node (the blue line) and *MoleBLEND* (the orange line) on the EU0 task of QM9, with the training set MAE serving as the metric.

C Ablation Studies

C.1 Noisy-node v.s. *MoleBLEND*

Figure 3 presents the training curves of Noisy-Node (represented by the blue line) and *MoleBLEND* (represented by the orange line) on the EU0 task of QM9. The X-axis shows the training steps, while the Y-axis shows the MAE of the training set. The graph reveals that Noisy-Node (the blue line) converges much faster than *MoleBLEND* at the beginning of training. However, as training progresses, *MoleBLEND* outperforms Noisy-Node. This finding suggests that pure 3D pretraining method (Noisy-Node) tend to learn representations that are closer to the 3D space, leading to quick convergence on 3D tasks. Nonetheless, incorporating both 2D and 3D information (*MoleBLEND*) yields better overall performance.

C.2 2D tasks with 3D information

Since our model is pretrained to predict both 2D and 3D information, for 2D tasks, we consider utilizing the 3D information predicted by our model as supplementary information (2D + 3D in Table 10). We observe that both settings achieve comparable performance across various tasks. This may be due to the 2D and 3D spaces have been well aligned and 3D knowledge is implicit injected into the model, allowing it to achieve satisfactory results even with only 2D information provided.

Table 10: Ablation studies on finetuning settings of 2D tasks.

Finetuning Settings	BBBP \uparrow	Tox21 \uparrow	ToxCast \uparrow	ClinTox \uparrow	Bace \uparrow	ESOL \downarrow	FreeSolv \downarrow	Lipo \downarrow
2D	73.0	77.8	66.1	87.6	83.7	0.831	1.910	0.638
2D + 3D	71.8	76.8	67.4	90.9	84.3	0.874	1.824	0.636